current understanding of human population substructure and genetic differentiation inferred from extensive anthropological sampling of blood groups and enzymes.

All of these approaches, even the first, require information about actual allele frequency distributions in a wide variety of ethnic subgroups that are likely to be relevant in forensic applications. Without the type of subpopulation studies already carried out for blood groups and enzymes, estimates of the probability of a matching DNA profile based on VNTR data, as currently calculated, are unjustified and generally unreliable.

REFERENCES AND NOTES

1. J. E. Hoover, in *The Encyclopedia Americana* (Grolier, Danbury, CT, 1982), pp. 215–219.
2. Identical twins and other monozygotic multiple births are obvious potential exceptions.
3. Y. Nakamura *et al.*, *Science* **235**, 1616 (1987).
4. E. S. Lander, *Nature* **339**, 501 (1989).
5. ———, *Am. J. Human Genet.* **49**, 899 (1991).
6. A. J. Jeffreys, V. Wilson, S. L. Thein, *Nature* **316**, 76 (1985).
7. B. Budowle *et al.*, *Am. J. Hum. Genet.* **48**, 841 (1991).
8. The importance of uniform and rigorously controlled laboratory standards is exemplified by tests carried out in the FBI Forensic Laboratory with DNA prepared from blood samples of 225 FBI agents. When the DNA typing was done twice in the same laboratory using slightly different procedures, 16% of the samples failed to agree in the two tests, including some individuals classified as homozygous in one test and heterozygous in the other. See (*11*).
9. Office of Technology Assessment, *Genetic Witness: Forensic Uses of DNA Tests* (U.S. Government Printing Office, Washington, D.C., 1990).
10. For example, if there is free recombination and 50% endogamy, then the proportion of the initial linkage disequilibrium that remains in successive generations follows the series 3/4, 9/16, 27/64, and so on; if the population had 80% endogamy, 2/3 of the original linkage disequilibrium would still be present after four generations.
11. *U.S. v. Yee*, 129 Federal Rules Decisions 629 (Northern District of Ohio) (1990).
12. R. Chakraborty and S. P. Daiger, *Hum. Biol.* **63**, 571 (1991).
13. R. Chakraborty, *Am. J. Human Genet.* **49**, 895 (1991).
14. To illustrate with a specific example, suppose a census population consists of a 9:1 mixture of two subpopulations with frequencies of an allele A of 0.5 and 0.9, respectively, and that each subpopulation mates randomly within itself. Then the excess of homozygotes in the census population is only 2.88% as compared with HWE, which would require a sample size of 1160 or larger to have a better than 50% chance of being detected by the conventional chi-square test. In contrast, a sample of only 11 individuals from each subpopulation would ensure a 50% chance of obtaining statistical significance in a chi-square test of the difference between the allele frequencies themselves.
15. A. E. Mourant, *The Distribution of Human Blood Groups* (Blackwell, Oxford, 1954).
16. ———, A. C. Kopec, K. Domaniewska-Sobczak, *The Distribution of Human Blood Groups and Other Polymorphisms* (Oxford Univ. Press, New York, 1976).
17. C. T. Caskey, *Am. J. Human Genet.* **49**, 893 (1991).
18. R. C. Lewontin, *Evol. Biol.* **6**, 381 (1972).
19. L. Nelson, *Am. J. Sociol.* **48**, 585 (1943).
20. R. J. R. Kennedy, *ibid.* **49**, 331 (1944).
21. ———, *ibid.* **58**, 56 (1952).
22. S. Lieberson, *Ethnic Patterns in American Cities* (Free Press, New York, 1962).
23. C. Peach, *Ethnic Segregation in Cities* (Univ. of Georgia Press, Athens, GA, 1981).
24. J. N. Spuhler and P. J. Clark, *Human Biol.* **33**, 223 (1961).
25. There is also the view that, because the true probability of a match at multiple VNTR bands will often be small, any estimate that is small will serve for courtroom purposes, even if the theoretical calculations are unjustified or if the reference database is faulty (*11*). The mistake here is to suppose that the true probability of a match is small when, in fact, it is unknown.
26. I. Balazs, *et al.*, *Am. J. Hum. Genet.* **44**, 182 (1989).
27. J. R. Kidd *et al.*, *Human Biol.* (1991).
28. On the other hand, it is unlikely that such loci will be found among the highly variable, and therefore, most informative, loci. Differentiation among subgroups is expected to be particularly pronounced for loci with large numbers of alleles, each in low frequency, especially in species like humans whose evolutionary history has mostly occurred in small, isolated local populations.
29. B. Budowle *et al.*, *Crim Lab. Digest* **18**, 9 (1991).
30. R. T. Acton *et al.*, in *Proceedings of the International Symposium on Human Identification 1989: Data Acquisition and Statistical Analysis for DNA Typing Laboratories* (Promega Corporation, Madison, WI, 1990), pp. 5–20.

Oscillatory Kinetics and Spatio-Temporal Self-Organization in Reactions at Solid Surfaces

GERHARD ERTL

Chemical reactions far from equilibrium on solid surfaces may exhibit typical phenomena of nonlinear dynamics, as exemplified by the catalytic oxidation of carbon monoxide on a platinum(110) single-crystal surface. Depending on the external parameters (temperature and partial pressures of the reactants), the temporal variation of the reaction rate may become oscillatory or even chaotic. In a parallel way, the concentration distributions of the adsorbed species on the surface form spatio-temporal patterns including propagating and standing waves, rotating spirals, as well as irregular and rapidly changing structures denoted "chemical turbulence."

IF A CHEMICAL REACTION IS OPERATED UNDER FLOW CONDITIONS with fixed external parameters, it will usually also exhibit a constant, steady-state rate of product formation. In certain cases, however, the response of the system may vary periodically or aperiodically with time. The most famous example is offered by the Belousov-Zhabotinsky (BZ) reaction in well-stirred homogeneous solution (*1*), in which periodic color changes reflect varying composition. Apart from other homogeneous reactions (*2*), certain heterogeneous processes occurring at gas-solid or liquid-solid interfaces were also found to exhibit such phenomena of temporal self-organization. These comprise electrochemical systems (*3*) as well as heterogeneously catalyzed reactions, either occurring with "real" catalysts near atmospheric pressure (*4*) or under ultrahigh vacuum conditions with well-defined single-crystal surfaces (*5*).

As an example (*6*), the variation of the potential U can be shown

The author is at the Fritz-Haber-Institut der Max-Planck-Gesellschaft, Faradayweg 4-6, W-1000 Berlin 33, Federal Republic of Germany.

as a function of time (Fig. 1) for an electrochemical system consisting of a Pt wire as the working electrode in a solution containing dissolved H_2 and Cu^{2+} (as well as Cl^- and ClO_4^-) ions. A constant current j flows through the cell, causing the reactions

$$H_2 \rightarrow 2H^+ + 2e^- \quad (1)$$

$$Cu^{2+} + 2e^- \leftrightarrows Cu \quad (2)$$

For small values of the current density j, the potential U adjusts to a constant stationary value (Fig. 1A) but starts to oscillate with a small amplitude (Fig. 1B) that grows further with increasing j (Fig. 1C). At j = 92 μA (Fig. 1D) another qualitative change (bifurcation) occurs, distinguished by alternating smaller and larger amplitudes. This first "period doubling" is followed by a second one (Fig. 1E), until for j = 126 μA the time series becomes aperiodic. This is an example of experimental verification of a transition from a stationary state through a series of period doublings to a chaotic state (Feigenbaum scenario) by stepwise variation of the external control parameter j (7). In fact, in this case, the chaotic state (Fig. 1F) can even undergo a further qualitative change to another chaotic state (Fig. 1G)—a transition denoted "interior crisis" (*8*).

The formal reason for such effects has to be sought in the mathematical structure of the equations that model the temporal behavior of the concentrations $\mathbf{u} = u_1, u_2, \ldots, u_i$ of the species involved in the reaction, which are nonlinear, coupled, ordinary differential equations, namely

$$\frac{d\mathbf{u}}{dt} = f(\mathbf{u}) \quad (3)$$

The nonlinear function $f(\mathbf{u})$ depends on the external control parameters (such as the current density j and the ion concentrations in the preceding example) and on the kinetics of the individual reaction-steps in the overall reaction. In fact, this approach represents a type of mean field approximation that assumes random spatial distribution of the reacting particles; that is, it neglects any specific interactions. Even more important, however, is the underlying assumption that the concentrations $\mathbf{u}$ depend solely on time, a condition that can be achieved experimentally by, for example, sufficiently rapid stirring of a solution. Otherwise, phenomena of spatio-temporal pattern formation would occur that have to be described theoretically by extending Eq. 3 into reaction-diffusion equations, as will be outlined below.

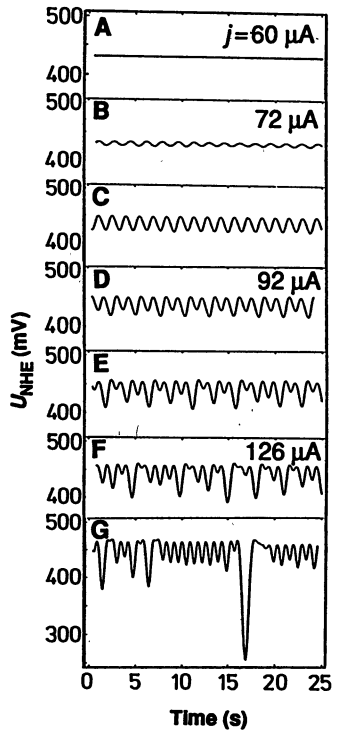

Fig. 1. Variation of the potential U of a Pt electrode under galvanostatic conditions at varying current densities j (increasing from **A** to **G**) in an aqueous solution with 1 M $HClO_4$, 1.5×10^{-4} M Cu^{2+}, and 5×10^{-4} M Cl^-; the solution is saturated with dissolved H_2 (NHE = normal hydrogen electrode) (*6*).

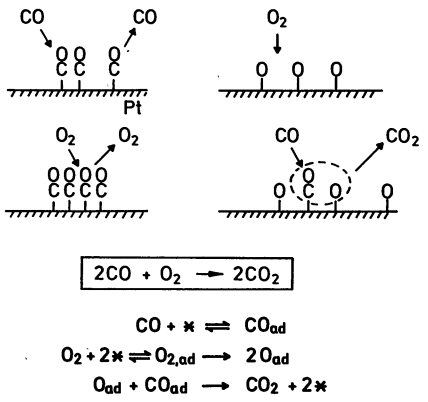

Fig. 2. Schematic mechanism of the reaction $2CO + O_2 \rightarrow CO_2$ on Pt surfaces. The symbol (*) denotes a free site on the surface.

Specification of the function $f(\mathbf{u})$ requires a detailed elucidation of the mechanism underlying the reaction studied, which may be rather complex: With the BZ system about 20 individual reaction steps are involved. However, for successful mathematical modeling these steps could be reduced to a much smaller set of effective variables (*9*). With the electrochemical reaction just presented, competition for free sites on the Pt surface between the H_2 molecules to be oxidized, the Cu^{2+} ions, and the anions acting as inhibitors is of importance, although the detailed mechanism has not yet been elucidated. In this article we concentrate on a conceptually simple reaction, the catalytic oxidation of CO on a Pt(110) single-crystal surface under low-pressure, isothermal conditions; the underlying elementary steps of this process have been analyzed in great detail and exhibit the full richness of oscillatory kinetics as well as of spatio-temporal self-organization.

Oscillatory Kinetics in the Catalytic Oxidation of CO on Pt(110)

The mechanism of the reaction $2CO + O_2 \rightarrow 2\ CO_2$ as catalyzed by surfaces of the Pt group metals has been well established (*10*) (Fig. 2). The two components to be adsorbed compete for the free sites on the surface, with a major difference, however: For dissociative chemisorption of O_2, a fairly large ensemble of neighboring unoccupied surface atoms is required, and adsorbed CO acts as an inhibitor for oxygen adsorption. The adsorbed O atoms O_{ad}, on the other hand, form a relatively open adlayer into which adsorption of CO is still possible. Thus, there is not substantial influence of preadsorbed oxygen on the adsorption probability for CO. The formation of CO_2 proceeds through recombination of CO_{ad} with O_{ad}, which is followed by immediate release into the gas phase, and within the framework of a mean field–type continuum description, the reaction rate can hence be simply formulated as $R = k_r u_1 u_2$, where u_1 and u_2 denote the surface concentrations (coverages) of adsorbed CO and O, respectively, and $k_r(T)$ is the rate constant for the surface recombination reaction (T = temperature). The state variables u_1 and u_2 are in turn determined by the sequence of reaction steps as

$$\frac{du_1}{dt} = s(\mathrm{CO})p_{\mathrm{CO}} - k_d u_1 - k_r u_1 u_2 \quad (4)$$

$$\frac{du_2}{dt} = s(\mathrm{O_2})p_{\mathrm{O_2}} - k_r u_1 u_2 \quad (5)$$

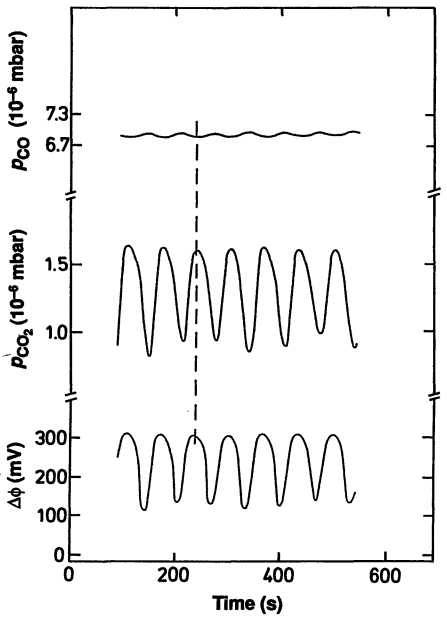

Fig. 3. Oscillatory kinetics with the catalytic CO oxidation at a Pt(110) surface. The recorded CO_2 partial pressure p_{CO_2} is proportional to the reaction rate; the work function change $\Delta\phi$ parallels the oxygen coverage u_2. (T = 480 K, $p_{O_2} = 2.1 \times 10^{-4}$ mbar, and $p_{CO} = 6.8 \times 10^{-5}$ mbar).

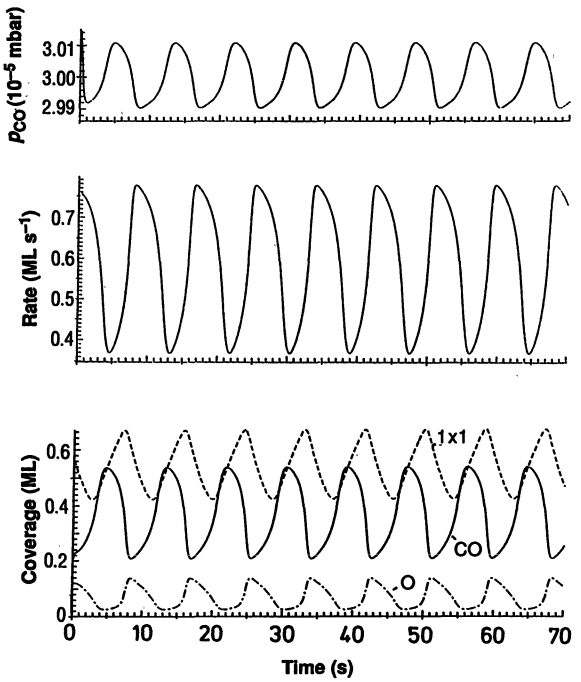

Fig. 5. Time series resulting from numerical integration of the three coupled differential equations modeling the kinetics of CO oxidation on Pt(110) for a particular set of control parameters (T = 540 K, $p_{O_2} = 6.7 \times 10^{-5}$ mbar, and $p_{CO} = 3.0 \times 10^{-5}$ mbar; ML = monolayer).

where $s(CO)$ and $s(O_2)$ are the sticking probabilities for adsorption of CO and O_2 (normalized to the impingement rates from the gas phase as determined by the partial pressures p_{CO} and p_{O_2}) and $k_d(T)$ is the rate constant for CO desorption. Thermal desorption of oxygen can be neglected at the temperatures of interest. The sticking probabilities $s(CO)$ and $s(O_2)$ are in turn functions of u_1 and u_2, reflecting the just-mentioned effects of site blocking. Hence, the kinetics are described by a set of nonlinear ordinary differential equations for the state variables u_1 and u_2, the solutions of which depend on the control parameters p_{CO}, p_{O_2}, and T.

With the Pt(110) surface, if operated under strictly isothermic low-pressure conditions, the reaction rate for a narrow range of control parameters is in fact not stationary but becomes oscillatory (*11*) (Fig. 3), as does the variation of the work function, $\Delta\phi$, and that of p_{CO}. The quantity $\Delta\phi$ is proportional to the oxygen coverage, u_2, and parallels the reaction rate. This reflects the fact that with this system kinetic oscillations are confined to conditions under which adsorption of oxygen is rate-limiting. This observation is in turn the key for rationalizing the physical mechanism underlying these phenomena as follows.

The clean Pt(110) surface does not in fact exhibit the atomic configuration that would correspond to the bulk termination (1 × 1, see Fig. 4) but is reconstructed into a "missing row" 1 × 2 structure that is energetically more stable. On the other hand, the heat of adsorption of CO on the 1 × 1 phase exceeds that on the 1 × 2 phase, and as a consequence a 1 × 2 → 1 × 1 transformation [by homogeneous nucleation and small local displacements of Pt atoms in the topmost layer (*12*)] takes place as soon as the CO coverage exceeds a critical value of about $u_{1,crit} = 0.2$ (*13*). The 1 × 1 phase exhibits, on the other hand, a higher oxygen sticking probability than the 1 × 2 phase; hence, for a narrow range of control parameters the surface structure will continuously switch between states of low (1 × 2) and high (1 × 1) reactivity. For mathematical formulation a third variable u_3 (the fraction of the surface area present as 1 × 1 phase) denoting the state of the surface has to be introduced, which enters into the oxygen sticking probability of Eq. 5 and is in turn determined by the CO coverage u_1. A series of typical time series resulting from numerical integration of this set of three coupled equations has been calculated (Fig. 5) (*14*). All input parameters were taken from independent experimental measurements. The qualitative agreement with the data of Fig. 3 is remarkable. (Differences in the time scale have to be attributed to the differing temperatures). Nevertheless, this model represents only an approximation and is thus not able to reproduce all the experimentally observed features characterizing the nonlinear dynamics of this system.

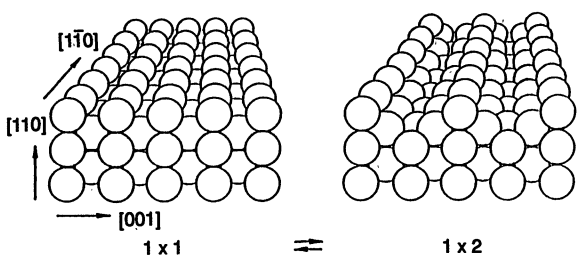

Fig. 4. The two structural modifications of the Pt(110) surface.

As in the electrochemical reaction presented in the introduction, the CO system may again undergo a transition from regular harmonic oscillations to chaotic temporal behavior through a sequence of period doublings during stepwise variation of one of the control parameters (*15*). One can illustrate this effect by converting the experimentally recorded time series into the so-called phase portraits by applying the time-delay method (*16*). Here the signal at time t, $x(t)$, is plotted versus $x(t + \tau)$, where τ is an arbitrarily chosen but fixed delay time. A harmonic periodic time series is thus converted into a single closed loop (Fig. 6A). Time series after the first and second period-doubling bifurcations are accordingly characterized by two and four loops (Fig. 6, B and C, respectively). The widths of these loops reflect the scatter in the experimental data, but within these limits the temporal behavior follows these "attractors" and is always clearly predictable. This predictability is no longer possible for the "strange" attractor for the chaotic state (Fig. 6D). The conditions underlying these results differ only by about 1% with respect to a single control parameter.

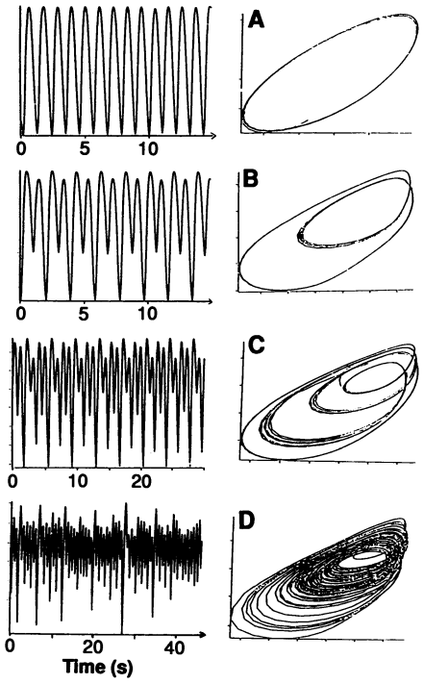

Fig. 6. Time series for the oscillatory CO oxidation on a Pt(110) surface (**left**) and corresponding phase portraits (**right**). Control parameters: T = 550 K, p_{O_2} = 4.0 × 10^{-4} mbar; (**A**) p_{CO} = 1.65 × 10^{-4} mbar, (**B**) p_{CO} = 1.62 × 10^{-4} mbar, (**C**) p_{CO} = 1.60 × 10^{-4} mbar, and (**D**) p_{CO} = 1.58 × 10^{-4} mbar.

Chaotic temporal behavior can be quantified by the Lyapounov exponents λ_i (*17*), which characterize the separation of adjacent points in phase space by proceeding along the variable x_i, that is, $e^{\lambda_i x_i}$. If all of the $\lambda_i \leq 0$, the trajectories in phase space will converge and stay together (Fig. 6, A through C). However, as soon as one of the λ_i becomes positive, even very small differences in the initial state will lead to divergence, and the system becomes chaotic (Fig. 6D). Recent detailed analysis of various chaotic time series from the CO system revealed that even two of the Lyapounov coefficients may become positive—a situation that is denoted "hyperchaos" and has so far not yet been identified with a chemical reaction (*18*).

Spatio-Temporal Pattern Formation

So far our discussion has been concerned with the temporal behavior of integral properties of chemical systems, such as the reaction rate, and the state variables u_i were assumed to depend solely on time. With a reaction in a homogeneous solution, such as the BZ reaction, these conditions may be realized by vigorous stirring, but with a heterogeneous reaction at a surface, "stirring" is not feasible. Generally, one has to conclude that with a macroscopic system the state variables depend also on spatial coordinates. As a reasonable approximation, such a system may be considered as consisting of subsystems, or cells, that are still large enough to justify the continuum concept of concentration variables u_i but that are small enough to ensure that within an individual subsystem the u_i are only time-dependent as given by the nonlinear kinetics of the reaction as expressed in Eq. 3. Concentration differences between adjacent cells will then give rise to transport processes, and Eq. 3 has to be extended accordingly into a set of partial differential equations of the type

$$\frac{\partial \mathbf{u}}{\partial t} = f(\mathbf{u}) + D\nabla^2\mathbf{u} \qquad (6)$$

which are known as reaction-diffusion equations (D = diffusion coefficient). Apart from diffusion as a consequence of the existence of concentration gradients, there may also be coupling between neighboring cells through heat conductance if the reaction conditions are nonisothermal and locally varying reaction rates give rise to temperature gradients. The latter effect is dominant, for example, with supported catalyst particles at higher pressures where the heat release by the exothermicity of the reaction together with a low heat conductance may give rise to substantial temperature changes (*19*). This effect will be of no importance with the system under discussion here; however, another global (that is, long-range) feedback mechanism may become relevant: As can be seen from Fig. 3, as a consequence of the varying reaction rate the partial pressures of the reactants are also subject to slight (<1%) modulations that are practically instantaneously ($\leq 10^{-4}$ s) effective everywhere on the catalyst surface.

The generic types of spatio-temporal patterns for extended systems modeled by reaction-diffusion equations in either bistable, excited, or oscillatory states have been widely studied theoretically (*20*) and have recently become accessible to experimental observation with the CO system as well.

Contrary to the BZ reaction in solution, for which concentration differences are easily made visible by color changes on the macroscopic scale, in the case of CO oxidation a more refined technique is required to display local variations in the coverages of adsorbed species. This can be achieved by application of a newly designed photoemission electron microscope (PEEM) (*21*). Because a chemisorption complex is associated with a dipole moment, local regions on the surface covered by different species will differ from each other with respect to their work function. As a consequence, irradiation

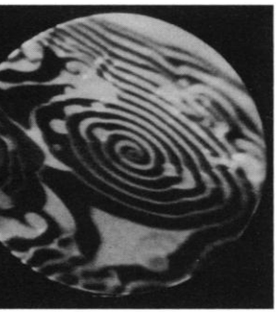

Fig. 8. Spiral wave pattern on Pt(110) as imaged by PEEM. T = 435 K, p_{CO} = 3.8 × 10^{-5} mbar, and p_{O_2} = 3.0 × 10^{-4} mbar. Diameter of the image is 0.4 mm.

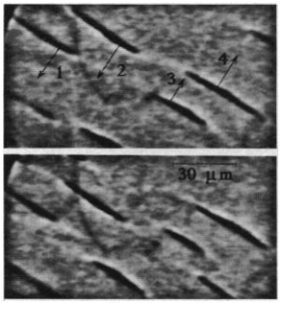

Fig. 7. Two PEEM images, recorded at an interval of 3 s, from a Pt(110) surface under steady-state CO oxidation conditions (T = 485 K, p_{CO} = 1 × 10^{-4} mbar, and p_{O_2} = 3.5 × 10^{-4} mbar). Dark regions with enhanced oxygen coverage propagate as solitary waves along the directions indicated.

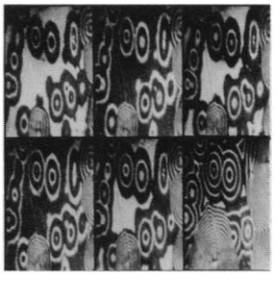

Fig. 9. A sequence of PEEM images from a 0.2 by 0.3 mm^2 section of a Pt(110) surface at T = 427 K, p_{CO} = 3 × 10^{-5} mbar, and p_{O_2} = 3.2 × 10^{-4} mbar (target patterns). The time interval between the last two images is 30 s, between the others it is 4.1 s.

with ultraviolet light gives rise to locally varying intensities of emitted electrons. The latter can be projected through a system of electrostatic lenses onto a fluorescent screen where they produce a gray-scale image that can be recorded by a charge-coupled device (CCD) camera and stored on videotape. In the present version the lateral and temporal resolutions are about 0.5 μm and 20 ms, respectively. In the images presented below, typically from a section of the surface 0.4 mm in diameter, oxygen-covered regions appear dark, and those covered by CO are bright.

For conditions outside the range of oscillatory kinetics, the system may be in a state of excitability that manifests itself in various types of propagating "chemical waves." Among these, solitary waves (Fig. 7) (*22*) are particularly remarkable. These are single-wave pulses with a bell-shaped profile propagating with constant speed of about 3 μm/s along the directions indicated by arrows that correspond to the crystallographic [001] orientation of the substrate Pt(110) surface. If two pulses traveling in opposite direction collide with each other, in most cases either one or both of them is annihilated, but in some cases the two waves emerge again with the same shapes and velocities. Phenomena of this type were first discovered with the numerical solution of a nonlinear wave equation from hydrodynamics (Korteweg–de Vries equation) and were denoted "solitons" (*23*). This name reflects the quasi-particle character of these events, which exhibit analogies to the nature of particles in quantum mechanics: After collision it cannot be decided if the wave pulses were reflected from each other or if they mutually penetrated and continued to propagate in their original direction—in other words, they become indistinguishable.

The most common spatio-temporal pattern of an excitable reaction-diffusion system is represented by continuously growing spirals (*2, 20, 24*), which have been extensively studied with the BZ reaction (*25*). An example of this type for the CO system is shown in Fig. 8 (*26*). The spiral wave is not circular but elliptic, with the long axis along the [110] direction and the short axis along the [001] direction of the substrate single crystal. This effect is due to the anisotropy of surface diffusion for adsorbed species, which affects the propagation velocities of the fronts of "chemical waves" (*27*); these velocities are 3.3 and 1.2 μm/s, respectively, in the two directions indicated.

Another type of pattern that may be formed if the control parameters are slightly changed so that the system becomes oscillatory is illustrated by the sequence of images in Fig. 9. These images exhibit concentric (again, elliptically shaped) waves emanating periodically with a frequency of about 0.15/s from nucleation centers ("pacemakers") from which they propagate with velocities of 4.2 and 1.5 μm/s, causing wavelengths of the order of 30 and 10 μm along [110] and [001], respectively. Again, such "target patterns" had been observed with the BZ reaction (*28*). Here, colliding wave fronts annihilate each other and lead, as a consequence, to cusplike structures as seen in Fig. 9. There are, in addition, features with much shorter wavelengths due to growing spirals, and the whole background switches periodically from bright (CO-covered) to dark (O-covered), signaling periodic ("mixed-mode") oscillations of the reaction rate integrated over the whole surface area. This periodic switching occurs fairly rapidly (<1 s) and has to be considered a manifestation of gas-phase coupling as an additional mechanism for spatial self-organization.

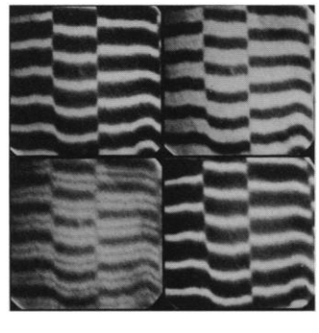

Fig. 10. Spatio-temporal patterns of the standing-wave type on a 0.3 by 0.3 mm^2 section of the Pt(110) surface, recorded in intervals of 0.5 s during harmonic kinetic oscillations of the type in Fig. 6A. T = 550 K, p_{O_2} = 4.1 × 10^{-4} mbar, and p_{CO} = 1.75 × 10^{-4} mbar.

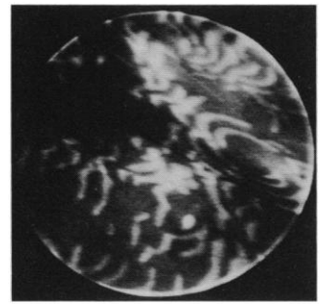

Fig. 11. Irregular and rapidly changing pattern (diameter 0.4 mm) characteristic of "chemical turbulence."

This latter global feedback process occurs practically instantaneously (~10^{-4} s), as outlined above, and dominates the synchronization underlying the kinetic oscillations occurring with high frequencies at more elevated temperatures. Regular rate oscillations, such as those in Fig. 6A, are associated with standing rather than propagating waves (Fig. 10). The whole macroscopic surface exhibits approximately equally spaced alternating dark and bright stripes, the intensities of which vary with the period of the associated kinetic oscillation. These spacings are not perfectly constant but may vary slightly even between neighboring pairs. As a consequence, dynamic "dislocations," as in Fig. 10, may be formed that only very slowly drift off.

The transition from regular kinetic oscillations to temporal chaos upon variation of one of the control parameters, as in Fig. 6, is accompanied by gradually increasing disorder in the spatio-temporal patterns. The orientations and spacings of the stripes become irregular, and finally they break up and no longer form standing waves but perform rapid motions. As can be seen in Fig. 11, these patterns are closely reminiscent of a turbulent fluid, and hence this state of spatio-temporal chaos may be denoted "chemical turbulence," although the underlying reaction-diffusion equations are of a mathematical structure quite different from the Navier-Stokes equations of hydrodynamics.

Conclusions

Phenomena of self-organization far from equilibrium are manifested in quite different areas, ranging from physics to sociology, and can be traced to common underlying principles of nonlinear dynamics (*29*). In addition, with chemical reactions occurring at solid surfaces, these effects are widespread (although frequently confined to narrow ranges of control parameters), and the number of systems for which kinetic oscillations and spatio-temporal pattern formation are observed will steadily grow. The main example presented here is of particular conceptual simplicity: The microscopic reaction steps are well established and allow modeling with few state variables. In addition, the system is genuinely two-dimensional and is not complicated by nonisothermal or convective processes. It may thus be considered a prototype for experimental verification and testing of the theoretical concepts of a fascinating and challenging field of research.

REFERENCES AND NOTES

1. A. M. Zhabotinsky, *Ber. Bunsenges. Phys. Chem.* **84**, 303 (1980); J. J. Tyson, *The Belousov-Zhabotinsky Reaction*, vol. 10 of *Lecture Notes on Biomathematics* (Springer-Verlag, Berlin, 1976).

2. R. Field and M. Burger, Eds., *Oscillations and Traveling Waves in Chemical Systems* (Wiley, New York, 1985).
3. U. F. Franck, *Ber. Bunsenges. Phys. Chem.* **84**, 334 (1980); J. L. Hudson and M. R. Bassett, *Rev. Chem. Eng.*, in press.
4. F. Razón and R. A. Schmitz, *Catal. Rev.* **28**, 89 (1986).
5. R. Imbihl, in *Optimal Structures in Heterogeneous Reaction Systems*, P. J. Plath, Ed. (Springer-Verlag, Heidelberg, 1989), p. 26; G. Ertl, *Adv. Catal.* **37**, 213 (1990).
6. K. Krischer, M. Lübke, W. Wolf, M. Eiswirth, G. Ertl, *Ber. Bunsenges. Phys. Chem.* **95**, 820 (1991).
7. M. J. Feigenbaum, *J. Stat. Phys.* **19**, 25 (1978).
8. C. Gregobi, E. Ott, J. A. Yorke, *Physica D* **7**, 181 (1983).
9. R. J. Field and R. M. Noyes, *J. Chem. Phys.* **60**, 1877 (1974); M. Eiswirth, A. Freund, J. Ross, *Adv. Chem. Phys.* **80**, 127 (1991).
10. T. Engel and G. Ertl, *Adv. Catal.* **28**, 1 (1979).
11. M. Eiswirth and G. Ertl, *Surf. Sci.* **177**, 90 (1986); M. Eiswirth, P. Möller, K. Wetzl, R. Imbihl, G. Ertl, *J. Chem. Phys.* **90**, 510 (1989).
12. T. Gritsch, D. Coulman, R. J. Behm, G. Ertl, *Phys. Rev. Lett.* **63**, 1086 (1989).
13. S. R. Bare, P. Hofmann, D. A. King, *Surf. Sci.* **144**, 347 (1984); T. E. Jackman, J. A. Davies, D. P. Jackson, W. N. Unertl, P. R. Norton, *ibid.* **120**, 389 (1982); R. Imbihl, S. Ladas, G. Ertl, *ibid.* **206**, L903 (1988).
14. K. Krischer, M. Eiswirth, G. Ertl, in preparation. A preliminary report is given in *Surf. Sci.* **251/252**, 900 (1991).
15. K. Krischer, M. Eiswirth, G. Ertl, *ibid.* **202**, 565 (1988).
16. F. Takens, in *Dynamical Systems and Turbulence*, D. A. Rond and L. S. Young, Eds. (Springer-Verlag, Heidelberg, 1981), p. 336.
17. V. I. Oseledec, *Moscow Math. Soc. Trans.* **19**, 197 (1968); H. Haken, *Advanced Synergetics* (Springer-Verlag, Heidelberg, 1983); A. Wolf, J. B. Swift, H. L. Swinney, J. A. Vastano, *Physica D* **16**, 285 (1985).
18. M. Eiswirth, Th. -M. Kruel, G. Ertl, F. W. Schneider, in preparation.
19. J. R. Brown, G. A. O'Netto, R. A. Schmitz, in *Temporal Order*, L. Rensing and N. I. Jaeger, Eds. (Springer-Verlag, Berlin, 1985), p. 86; R. Sant and E. E. Wolf, *J. Catal.* **110**, 249 (1988); F. Schüth, X. Song, L. D. Schmidt, E. Wicke, *J. Chem. Phys.* **92**, 745 (1990).
20. A. S. Mikhailov, *Foundations of Synergetics I: Distributed Active Systems* (Springer-Verlag, Berlin, 1990).
21. W. Engel, M. Kordesch, H. H. Rotermund, S. Kubala, A. von Oertzen, *Ultramicroscopy* **36**, 148 (1991).
22. H. H. Rotermund, S. Jakubith, A. von Oertzen, G. Ertl, *Phys. Rev. Lett.* **66**, 3083 (1991).
23. N. Zabusky and M. D. Kruskal, *ibid.* **15**, 240 (1965).
24. Y. Kuramoto, *Chemical Oscillations, Waves and Turbulence* (Springer-Verlag, Berlin, 1984).
25. A. T. Winfree, *Science* **175**, 634 (1972); *Sci. Am.* **230**, 82 (June 1974); J. J. Tyson and J. P. Keener, *Physica D* **21**, 307 (1986); *ibid.* **32**, 327 (1988); P. Foerster, S. C. Müller, B. Hess, *Science* **241**, 685 (1988).
26. S. Jakubith, H. H. Rotermund, W. Engel, A. von Oertzen, G. Ertl, *Phys. Rev. Lett.* **65**, 3013 (1990).
27. J. Ross, S. C. Müller, C. Vidal, *Science* **240**, 460 (1988); R. Arnold, K. Showalter, J. Tyson, *J. Chem. Educ.* **64**, 740 (1987).
28. A. N. Zaikin and A. M. Zhabotinskii, *Nature* **225**, 535 (1970).
29. H. Haken, *Synergetics—An Introduction* (Springer-Verlag, Berlin, 1978); G. Nicolis and I. Prigogine, *Self-Organization in Nonequilibrium Systems* (Wiley, New York, 1977); R. Feistel and W. Ebeling, *Evolution of Complex Systems* (D. Reidel, Berlin, 1989).